

Article

Influence of Laser-Assisted Fusing on Microstructural Evolution and Tribological Properties of NiWCrSiB Coating

Changkyoo Park ¹ and Eun-Joon Chun ^{2,*} 

¹ Laser and Electron Beam Application Department, Korea Institute of Machinery and Materials, Daejeon 34103, Korea; ck0421@kimm.re.kr

² Department of Nano Materials Science and Engineering, Kyungnam University, Changwon 51767, Korea

* Correspondence: ejchun@kyungnam.ac.kr; Tel.: +82-55-249-2695

Received: 5 April 2020; Accepted: 22 April 2020; Published: 23 April 2020



Abstract: The present study examines the applicability of a diode laser-assisted fusing treatment and a temperature-control system to the NiWCrSiB thermal spray coating to develop the enhanced wear resistance of continuous-casting molds. As a result of the use of the lasers, the variations in the microstructure and the hardening behavior during the fusing treatment could be controlled. Fine secondary phases (approximately 0.05–10 μm in size) homogeneously present in the coating after the laser-assisted fusing were observed to be Cr-, Mo- and W-based carbides and borides. Transmission electron microscope analysis was used to characterize these fine secondary phases as M_7C_3 and M_{23}C_6 carbides and M_5B_3 boride. Because of these fine secondary phases, the hardness increased from 730 (as-sprayed status) to 1230 HV (after fusing at a temperature of 1473 K). Finally, given the formation of fine secondary phases and the occurrence of surface hardening, the laser-assisted fusing treatment was deemed to enhance the tribological performance of the thermal-sprayed coating, in that it exhibited a lower coefficient of friction and lower wear rate than the as-sprayed coating.

Keywords: thermal spraying; laser-assisted fusing treatment; carbides; borides; wear

1. Introduction

Thermal spraying is a well-known and cost-effective surface-coating process. It is widely used to produce wear- and corrosion-resistant coatings in the chemical and machinery industries [1]. Typically, nickel (Ni)-based alloy powders containing alloying elements such as carbon (C), boron (B), tungsten (W), silicon (Si) and chromium (Cr) are used for thermal spraying. Among these, NiWCrSiB powder (called as 1276F) is commonly used to form a surface coating capable of resisting abrasion and erosion at high temperatures.

Throughout the steel production process, the production hardware is exposed to a combination of high temperatures, corrosive environments and wear. This demanding and severe environment gives rise to a broad range of degradation mechanisms and ultimately leads to a reduction in product quality, reduced operating efficiencies and high maintenance costs. [2,3]. Among the production hardware, continuous casting molds are exposed to particularly high-temperature and abrasive environments. As a result, large amounts of surface wear occur during long-term service of the casting molds [4]. Especially, the molds are crucial part to continuous-casting systems and the surface quality of these molds is highly correlated with the surface quality of the resulting slab. To ensure the production efficiency of a continuous-casting machine, high durability with a minimum of mold surface damage is essential. To this end, copper (Cu)-based molds were electroplated with Ni alloys and thermal spray coating with 1276F alloy was examined to achieve the further enhancement of surface mechanical

properties. However, since a thermal-sprayed layer commonly exhibits macrostructural inhomogeneity (e.g., the macrosegregation of specific elements and voids) after spraying, subsequent treatment, such as fusing within a certain temperature range, is essential to enhance the mechanical properties of the coating [5]. To this end, Otsubo et al. investigated the effects of fusing on the macro- and microstructural variation behaviors of several kinds of Ni-based alloy coatings [6,7]. Their studies revealed that a M_6C carbide, as well as M_7C_3 carbides and a M_3B_2 boride appeared, while the Ni/Ni₃B eutectic phase and voids disappeared from the coating after the fusing process. Sakata et al. also reported on microstructural variations as well as an enhancement of the wear resistance through the application of heat treatment to a cobalt (Co)-based alloy coating [8]. Fusing in a furnace is usually performed over a certain temperature range to achieve macrostructural homogeneity and enhanced mechanical properties, relative to the as-sprayed state. However, when a dissimilar combination of materials (as in the case of a continuous-casting mold with a Cu alloy plate and a thermal-sprayed Ni-based alloy layer) is used for the fusing treatment, desquamation of the thermal-sprayed layer has frequently been reported due to the distortion caused by the different thermal expansion coefficients of the thermal-sprayed layer and the substrate. That is, selective fusing of the thermal-sprayed layer is necessary to manufacture exceptionally durable continuous-casting molds with minimal distortion.

Laser-based processes are currently in widespread use for the surface modification of metallic alloys, because the selective control of the mechanical and chemical properties of the material at the local surface is possible. For instance, to improve the surface wear resistance, Houdková et al. attempted the laser-based surface remelting of a thermal-sprayed Co-based alloy [9]. Furthermore, Santhanakrishnan et al., Chun et al. and Shariff et al. reported on the surface hardening that could be attained by applying laser-based surface heat treatment to tool and plastic molds, as well as railroad steels, respectively [10–12]. Hongchao et al. also found that laser shock peening enhances the surface hardening behavior and fatigue resistance of titanium (Ti) alloys [13]. Clearly, the surface properties of materials can be controlled by applying these types of laser-based surface modification systems. Among these processes, a heat treatment technique with diode lasers for homogenization and phase transformation is widely applied to the fabrication of molds in various industrial fields. The process improves the wear and corrosion resistance of the molds that must be capable of long-term service in severe service environments. Especially, a diode laser has higher beam absorptivity for the metallic materials as compared with that of CO₂ [14], Nd: YAG [15] and fiber [16] lasers and a large area of sample can be treated by the rectangular beam shape with a flat top energy distribution. Thus, the heat treatment using a diode laser (i.e., laser-assisted fusing) could be regarded as a strong candidate for fusing a thermal-sprayed layer to develop the high-durability continuous-casting molds.

However, although several studies have addressed the fusing of thermal-sprayed Ni and Co-based powders, the fundamental applicability of temperature-controlled laser-assisted fusing and its influence on microstructural evolution and wear resistance remains still insufficient, especially for the 1276F coating. Giacomantonio et al. examined the effect of CO₂ laser-assisted fusing treatments (based on remelting concept) on the macrostructural homogenization behavior of Ni-based thermal-sprayed layer [17]. However, the treatment was performed without consistent temperature control and they did not elucidate the effect of the laser irradiation conditions on the microstructure and mechanical properties. In addition, the effect of laser-assisted fusing on the wear properties was not examined. Lugscheider et al. investigated laser-assisted fusing with a CO₂ laser for a Co-based coating, controlling the degree of fusing by adjusting only the laser power [18]. However, the temperature of the fusing treatment should be kept constant throughout the process to maximize the degree of fusing; merely controlling the laser power and remelting during the treatment may lead to temperature variations due to thermal storage. Especially, Chun et al. reported the fundamental results of laser-assisted fusing on 1276F coating [19]. However, they did not cover the characterization of microstructural change in detail. Furthermore, there was no report on variation of wear resistance upon the laser-assisted fusing, which was regarded as core property for the continuous casting mold.

In the present study, the applicability of a temperature-controlled laser-assisted fusing treatment was examined for a 1276F thermal-spray coating to develop a high-durability continuous casting mold. To this, microstructural evolution of a 1276F coating was characterized in detail and correlation between microstructural characteristics and wear resistance of the coating upon a laser-assisted fusing conditions was systematically studied.

2. Materials and Methods

2.1. Materials

A single type of commercial Ni-based powder (1276F) was employed for the thermal spraying. Its chemical composition is given in Table 1.

Table 1. Chemical compositions of Ni-based alloy powder used in the present study (mass %).

Materials	Ni	C	Cr	W	B	Si	Fe	Mo
1276F	Bal.	0.8	14.3	16.2	2.9	3.8	3.3	5.0

2.2. Methods

2.2.1. Thermal Spraying

The pure Cu sheet (thickness: 30 mm) was electroplated with pure Ni (thickness: 0.7 mm). Next, thermal spraying of the substrate (i.e., on the surface of the electroplated pure Ni layer) was performed using the high-velocity oxygen fuel (HVOF) method. The thermal spraying conditions are summarized in Table 2.

Table 2. Thermal spraying conditions (HVOF).

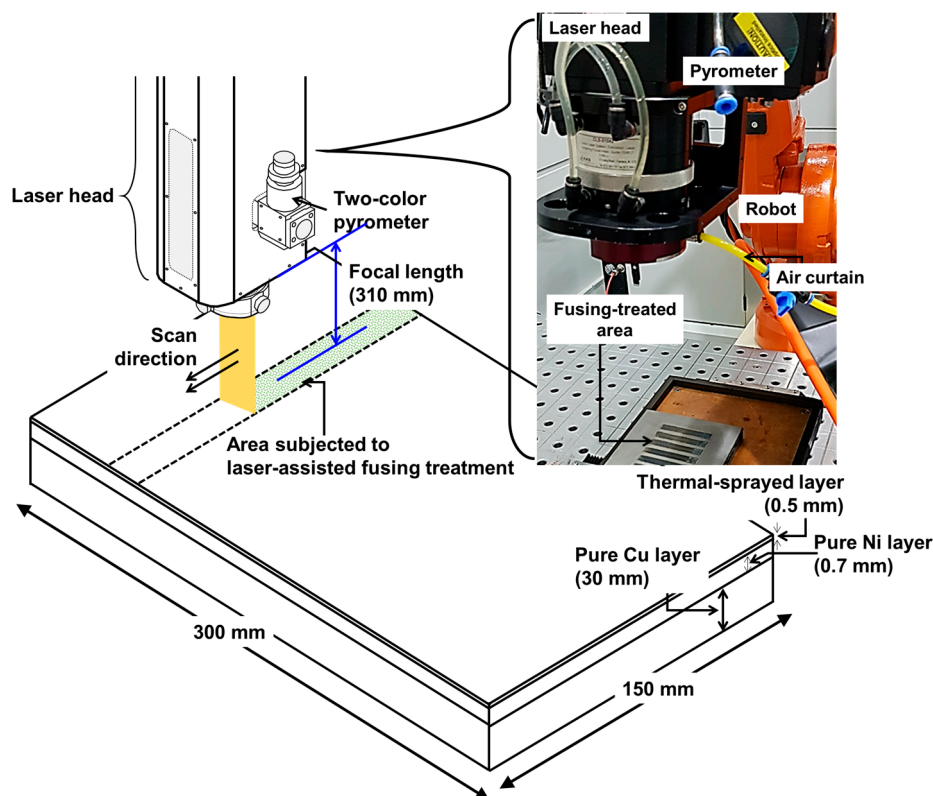
Parameter	Value
Thermal spray gun	JP-5000 [®] (TAFA Inc., Concord, CA, USA)
Powder flow rate (g/m)	70–100
Oxygen flow rate (ℓ/m)	1000–1200
Gasoline flow rate (ℓ/m)	3–5
Thickness of sprayed layer (mm)	0.17–0.2

2.2.2. Laser-Assisted Fusing Treatment

The thermal-sprayed specimens were subjected to fusing treatment using a diode laser system (4-kW TeraBlade laser, TeraDiode Inc., Wilmington, NC, USA). The key conditions for the laser-assisted fusing are listed in Table 3, while Figure 1 shows the laser-assisted fusing treatment system and specimen arrangement. The laser beam dimensions were 6 × 4 mm. Laser beam irradiation was performed with temperature control applied in real time. The laser power was automatically controlled to maintain the surface temperature during the treatment. To this end, to monitor the fusing treatment temperature at the specimen surface, a pyrometer (LASCON[®]) was positioned coaxially with the laser beam. The pyrometer was calibrated using a black body source. The laser head, together with the pyrometer system, was controlled by a six-axis robot. Prior to the fusing treatment, pre-heating of the thermal-sprayed specimen was also performed using an induction-heating device. The fusing treatment was performed over a temperature range of 1173–1473 K, with a laser scan speed of 1.0 mm/s.

Table 3. Laser-assisted fusing treatment conditions.

Parameter	Value
Oscillator	4-kW diode laser (TeraBlade Laser, TeraDiode Inc.)
Wavelength of laser beam (nm)	900–1070
Beam dimensions (mm)	6 × 4
Direction of laser beam irradiation	Perpendicular to specimen surface
Focal length (mm)	310
Defocus distance (mm)	0
Scan speed of laser beam (mm/s)	1.0
Fusing temperature (K)	1173–1473
Pre-heating temperature (K)	573 K

**Figure 1.** Experimental setup for laser-assisted fusing treatment and specimen arrangement.

2.2.3. Microstructure

The cross-sectional microstructure of the treated specimen was observed by optical microscopy (OM, Olympus, BX51M, Olympus, Tokyo, Japan,) and scanning electron microscopy (SEM, SNE-4500M, SEC, Suwon, Korea). The microstructure and elemental distribution in the treated zone were analyzed using an electron probe X-ray micro analyzer (EPMA, JXA-8530F, JEOL, Tokyo, Japan) and a transmission electron microscope (TEM, JEM-2100F, JEOL, Tokyo, Japan) with an energy-dispersive X-ray spectroscope (EDS, Inca X-sight, Oxford Instrument, Abingdon, UK). TEM samples were prepared using a multi-beam focused-ion beam (FIB) and a scanning electron microscope (SEM) system (LYRA 1 XMH, Tescan, Brno, Czech Republic), using an in situ lift-out method.

2.2.4. Surface Mechanical Properties

To confirm the effect of the fusing treatment conditions on the mechanical properties of the thermal-sprayed layer, Vickers hardness testing (MMT-X, Matsuzawa, Tokyo, Japan) was performed with a testing load of 0.25 N and a dwell time of 10 s. The influence of the laser-assisted fusing treatment on the tribological performance of the thermal-sprayed coating was evaluated using a pin-on-disk tribometer (CETR UMT-2, Bruker, Billerica, MA, USA). The size of the specimen was $10 \times 10 \times 5$ mm. This was pressed against a rotating cast iron disk with a diameter of 142 mm. Before attempting to measure the tribological properties, samples were burnished with SiC abrasive paper (PC221, Deerfos Co., #600 grit, Incheon, Korea) attached to the disk to ensure an even contact with the counter material. The tribotest was performed using SiC abrasive papers (PC221, Deerfos Co., #320 grit, Incheon, Korea) attached to the disk, sliding against the as-sprayed coating sample and that treated with the laser-assisted fusing. The new SiC abrasive paper was utilized at every 50 m of sliding distance. The tribotest was conducted with the following parameters; normal load = 30 N, sliding speed = 28.8 mm/s and total distance = 200 m (as listed in Table 4). The thickness of the samples was measured at every 50 m of sliding distance and the wear volume was estimated by multiplying the worn thickness by the area of the specimen. All the tribotests were repeated three times and the obtained wear losses were averaged. After the test, the surface morphology and elemental distribution of worn surface were observed and analyzed by SEM and EPMA, respectively. Moreover, the average surface roughness (Ra) and line profilometry of worn surface were analyzed by laser scanning microscopy (VK-8710, Keyence, Osaka, Japan) with a wavelength of 658 nm and depth resolution of 0.2 μm .

Table 4. Tribotest conditions.

Parameter	Value
Tribometer	Pin-on-disk type
Abrasive media	SiC abrasive paper (#320 grit)
Load (N)	30
Rotational speed (rpm)	5
Distance (m)	200

3. Metallurgical Basis for Determination of Laser-Assisted Fusing Treatment Conditions

3.1. Thermodynamic Calculations for Phase Fraction of 1276F Alloy

Figure 2 shows the thermodynamic calculation results explaining the relationship between the temperature and phase fraction for 1276F alloy, obtained using Thermo-Calc software (TCNI8 database). The primary matrix phase is gamma (γ), with carbide and boride secondary phases also present from 1300 to 1500 K. In the temperature range corresponding to the mushy zone of the Ni-based alloy powder, it was confirmed that the hardness of the treated zone was lower than that of the as-sprayed alloy, as was previously found by Chun et al. [20]. Hence, in this study, the temperature at which the treatment was applied was selected such that it would be within the solid status, that is, from 1323 to 1473 K. The fusing treatment temperature is also shown in Figure 2.

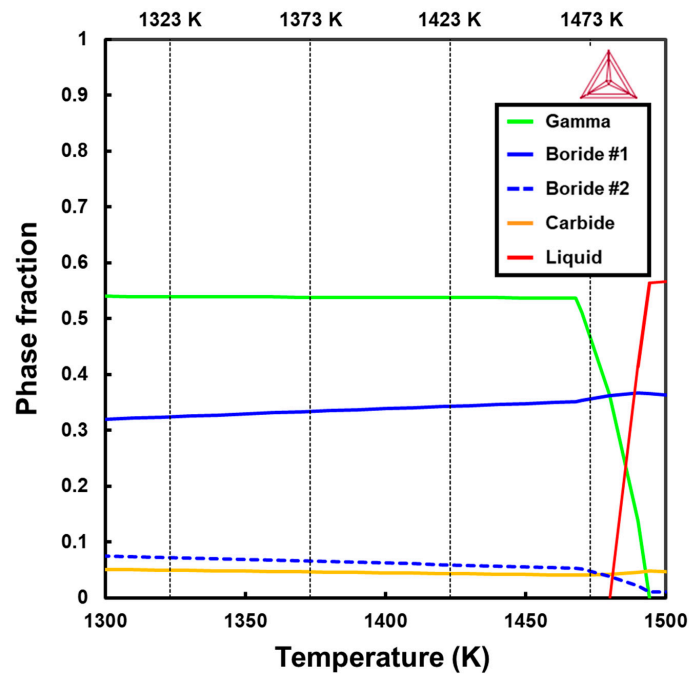


Figure 2. Thermodynamic calculations (Thermo-Calc) of phase fraction as a function of temperature for 1276F alloy.

3.2. Control of Surface Temperature and Laser Power during Laser-Assisted Fusing

Figure 3 shows the representative laser power and surface temperature history during the laser-assisted fusing treatment of the 1276F coating at 1373 K. The temperature obtained via thermodynamic calculation as explained in Section 3.1 was maintained by adjusting the laser power in real time. The laser power was approximately 0.9 kW at the beginning of the fusing treatment and then decreased to a stable 0.6 kW at this target temperature. Similar temperature and laser power trends were observed with other fusing-treatment conditions.

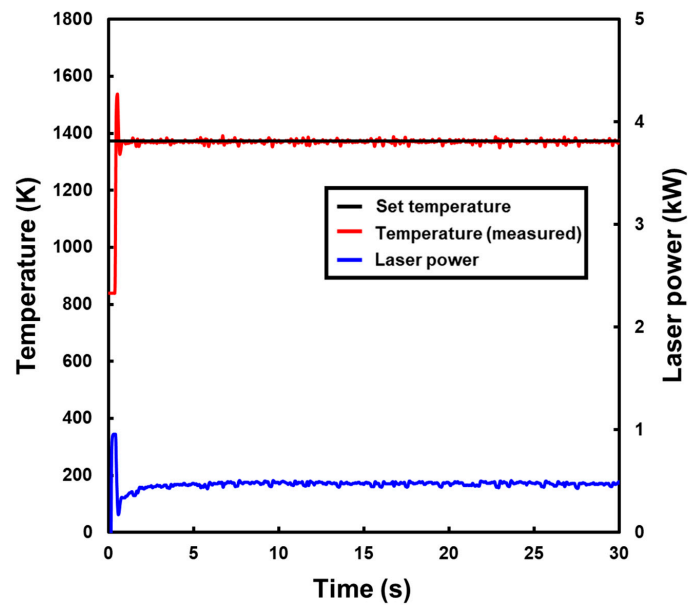


Figure 3. Laser power and temperature trends during laser-assisted fusing treatment of 1276F alloy (set temperature = 1373 K).

4. Effect of Laser Irradiation on Fusing Ability for 1276F Coating

4.1. Macrostructure and Element Distribution of As-Sprayed Coating

Figure 4 shows a representative optical cross-sectional macrostructure and the results of EPMA analysis for region A in Figure 4a for the as-sprayed state. As shown in Figure 4a, numerous voids are formed in the sprayed 1276F layer, while no cracks can be detected. Moreover, Mo and W are locally segregated (i.e., macrosegregated), as shown in Figure 4b and the carbides and borides are not homogeneously distributed. In addition, the microstructure distribution exhibited a wave-pattern. Thus, the as-sprayed specimen exhibits macro- and microstructural inhomogeneity, in terms of the presence of voids and the macrosegregation of the alloying elements.

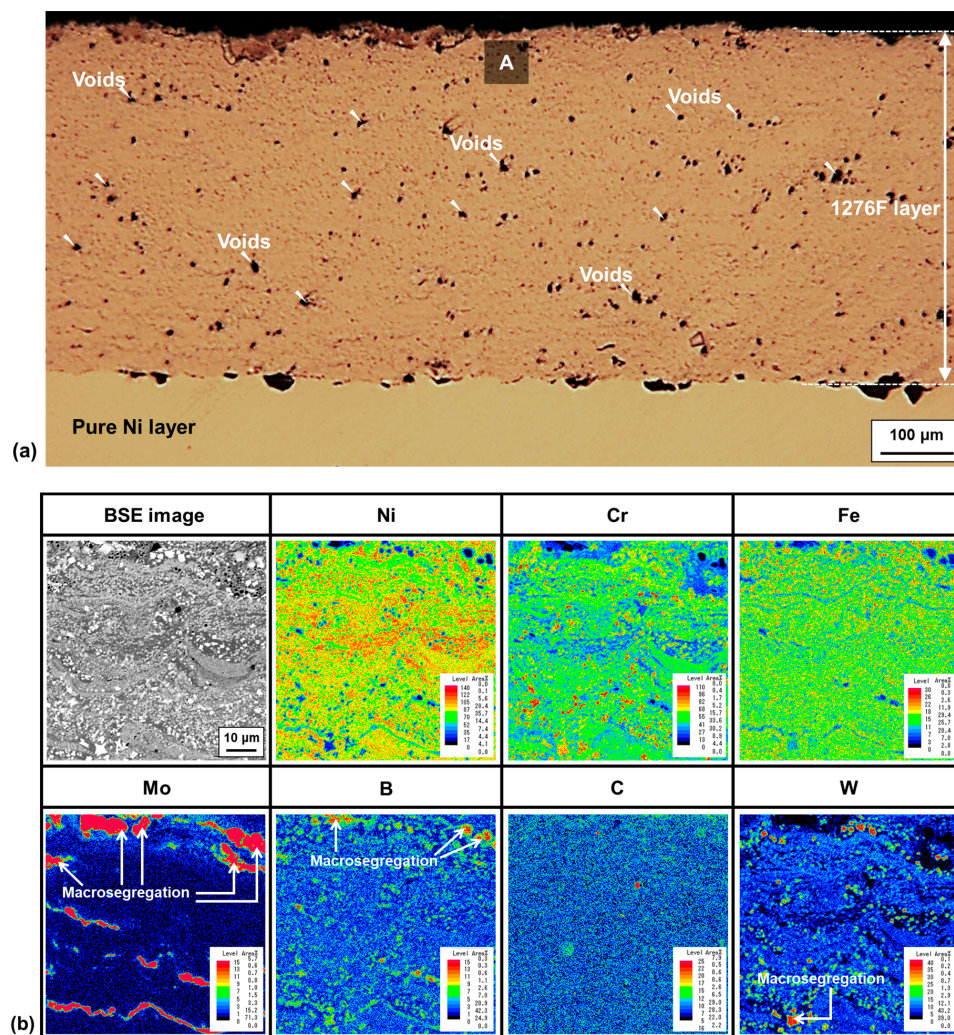


Figure 4. (a) Macrostructure and (b) element distribution obtained by EPMA analysis (from “A” region in (a)) of the thermal-sprayed layer of the as-sprayed specimen.

4.2. Homogenization Behavior upon Laser-Assisted Fusing Temperatures

Figure 5 shows a representative variation in the cross-sectional macrostructure to illustrate the homogenization behavior of the 1276F coating after the laser-assisted fusing treatment at 1173, 1323 and 1473 K. Compared with the as-sprayed coating, the fusing treated depth increases with the treatment temperature up to 1473 K. At a treatment temperature of 1473 K with a 1.0 mm/s scan speed, the 1276F coating could be fully fused. Furthermore, the number of voids is also reduced with an increase in the fusing temperature from 13% (as sprayed coating) to 0.3%. (the fusing treated coating at 1473 K).

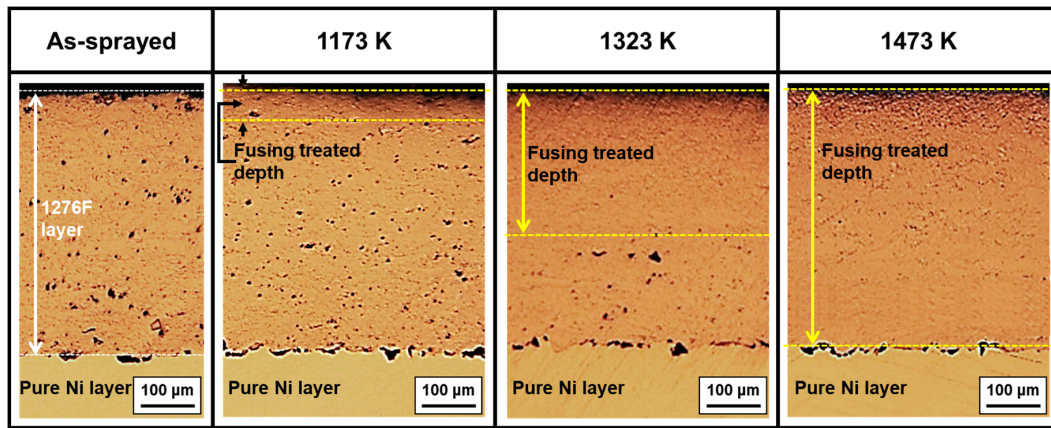


Figure 5. Variation in cross-sectional macrostructure as a function of fusing treatment temperature.

4.3. Relationship between Hardness and Microstructure upon Laser-Assisted Fusing Treatment

Figure 6 shows the hardness distribution from the top surface of the thermal-sprayed layer to the pure Ni layer for the 1276F alloy specimen at various fusing temperatures. The hardness was evaluated at the center of the region subjected to the laser-assisted fusing treatment (as also described in Figure 6). At a fusing temperature of 1173 K, a peak hardness of 1150 HV was observed near the surface (< 0.08 mm from the surface), which decreased towards the as-sprayed region (approximately 730 HV). In the fully fused condition (i.e., at 1473 K), the hardness ranged from 1103 to 1230 HV. Consequently, the treated depth shown in Figure 5 exhibits an enhanced level of hardness, relative to that of the as-sprayed specimen; hence, a reduction in the number of voids and an increase in the hardness through the application of the laser-assisted fusing treatment were confirmed for the 1276F coating layer.

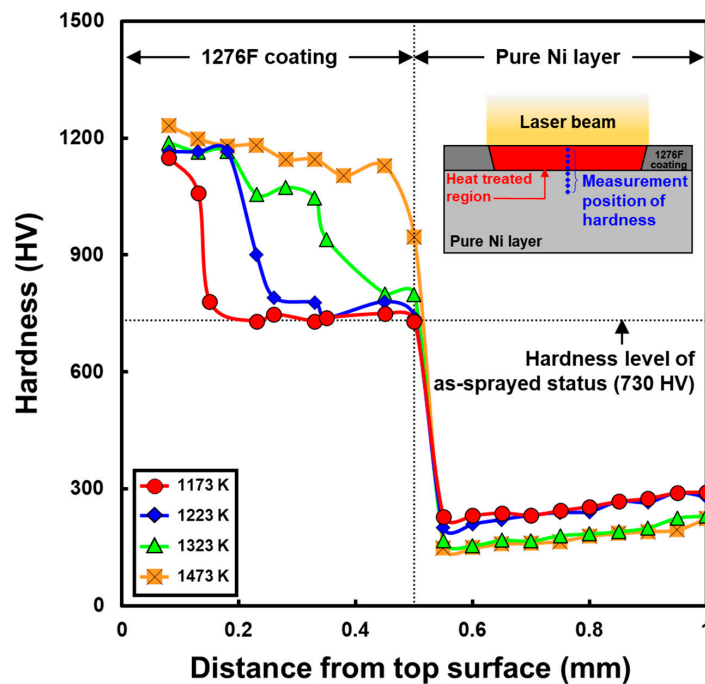


Figure 6. Hardness distribution of thermal-sprayed layer after laser-assisted fusing treatment.

Figure 7 shows a representative backscattered electron (BSE) image and elemental distributions obtained by electron probe X-ray micro analyzer (EPMA) near the surface of the thermal-sprayed layer after laser-assisted fusing at 1473 K. The microstructure after the treatment is clearly different from that

of the as-sprayed specimen (shown in Figure 4b). The zone subjected to the treatment consisted of finely distributed secondary phases (as revealed in the BSE images), while the as-sprayed zone did not (shown in Figure 4b). The Cr, Mo, W, C and B distribution maps revealed these fine secondary phases to be Cr, Mo and W-based carbides and borides. Their sizes ranged from approximately 0.05 to 10 μm .

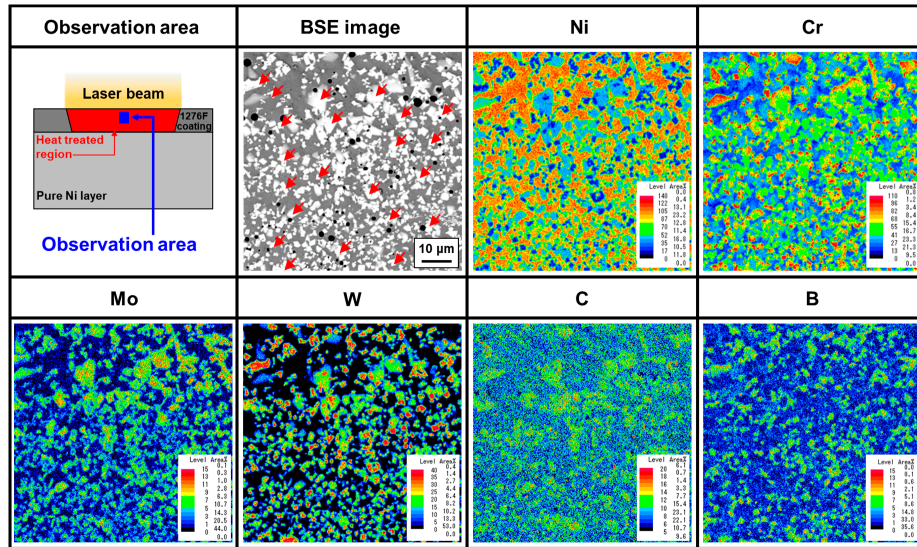


Figure 7. Electron probe X-ray micro analyzer (EPMA) analysis of thermal-sprayed layers after laser-assisted fusing treatment of 1276F coating at 1473 K (red-colored arrows in BSE image indicate secondary phases).

Figure 8 also shows typical bright field (BF) images and corresponding element maps analyzed by TEM for the fusing treated coating at 1473 K. The formation of Cr, W and Mo-based secondary phases based on a matrix phase consisting of Ni can be confirmed. Furthermore, as shown in Figure 9, the representative secondary phases after fusing at 1473 K were characterized as (a) M_7C_3 and (b) $M_{23}C_6$ carbides, as well as (c) M_5B_3 boride. Therefore, the hardness increment from 730 (as-sprayed) to 1230 HV (fused) after treatment at 1473 K (described in Section 4.3) can be ascribed to the presence of fine carbides (M_7C_3 , $M_{23}C_6$) and boride (M_5B_3) with the uniform distribution, which is not present in the as-sprayed layer (as displayed in Figure 4b).

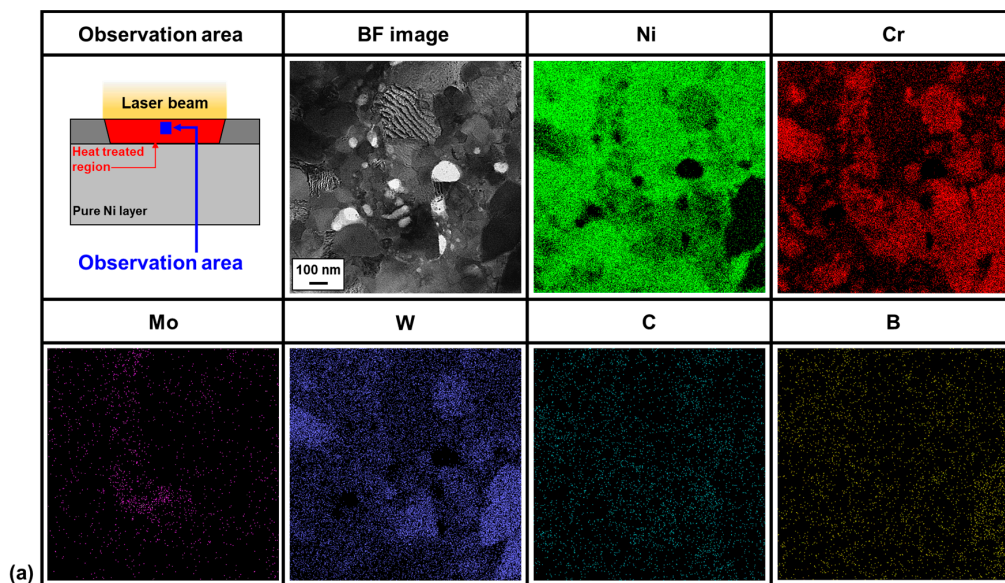


Figure 8. Cont.

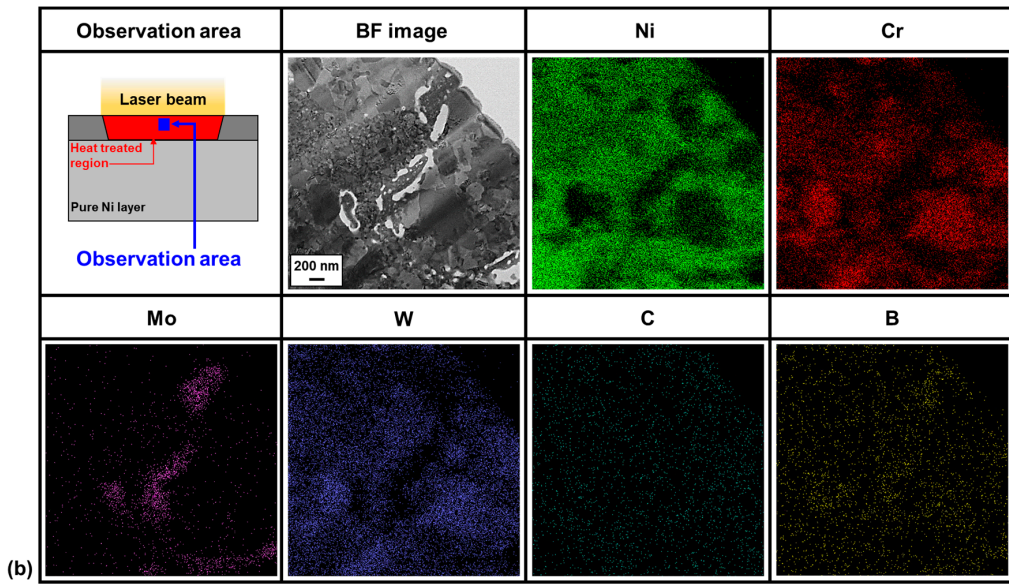


Figure 8. (a,b) BF image and EDS analysis of thermal-sprayed 1276F coating after laser-assisted fusing treatment at 1473 K.

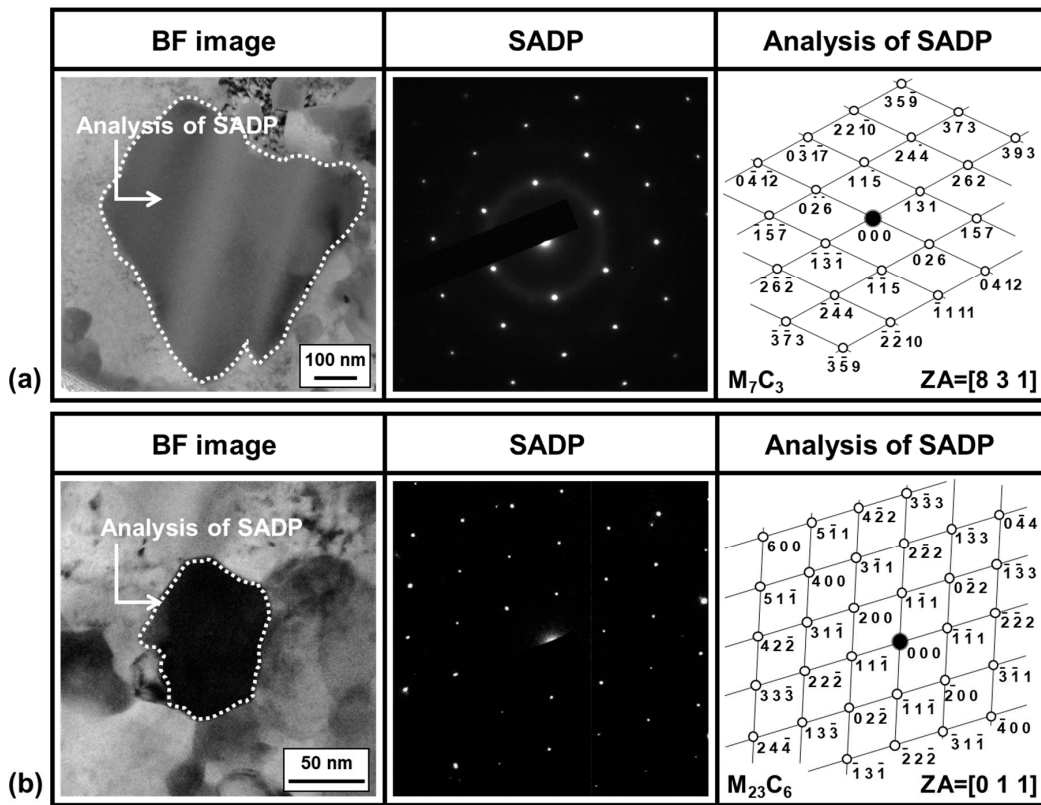


Figure 9. Cont.

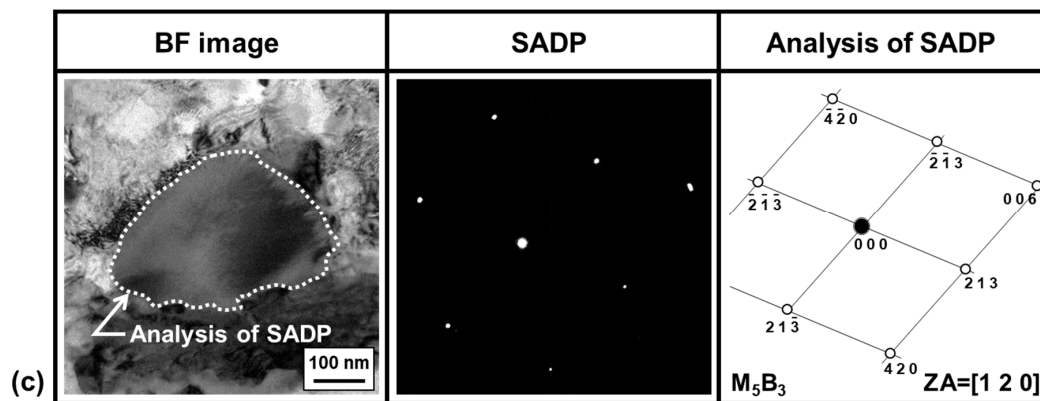


Figure 9. Bright field (BF) images and corresponding selected area diffraction pattern (SADP)-designated areas after laser-assisted fusing treatment of 1276F coating at 1473 K; (a) M_7C_3 , (b) $M_{23}C_6$ and (c) M_5B_3 phases.

5. Influence of Laser-Assisted Fusing on Tribological Properties of 1276F Coating

Figure 10 shows the variation in the coefficient of friction (COF) as a function of the sliding distance for the as-sprayed 1276F coating, as well as that of the coating after the laser-assisted fusing treatment at 1473 K. The COF of the as-sprayed coating was somewhat higher than that of the sample after treatment (average COF: 0.408 for the as-sprayed coating; 0.356 for the coating after treatment). Moreover, the variation in the COF value of the as-sprayed coating was somewhat larger than that of the laser-assisted fusing coating. In the case of the as-sprayed coating, the maximum COF (COF_{max}) value was 0.428 and the minimum COF (COF_{min}) value was 0.387 after the COF values reached the steady state. As a result, the difference between COF_{max} and COF_{min} was 0.041. On the other hand, in the case of the laser-assisted fusing treatment, the variation in the COF value was found to be 0.028 ($COF_{max} = 0.372$; $COF_{min} = 0.344$). This relatively larger variation in the COF value was attributed to the macrostructural inhomogeneity such as macrosegregation and voids in the as-sprayed coating. Figure 11 also compares the average wear rate, measured every 50 m, of the as-sprayed coating and the laser-assisted fusing coating. The error bars represent the range of wear rate. Given this result, we can say that the coating treated with laser-assisted fusing exhibits a relatively higher wear resistance than that of the as-sprayed coating. The wear rate of the laser-assisted fusing coating was 28% less than that of the as-sprayed coating at the 200-m point. Relatively softer material of the as-sprayed coating may be subjected to more severe plastic deformation in comparison to that of the laser-assisted fusing treatment, resulting in larger contact area friction force. Eventually, the relatively larger wear loss and COF values were obtained from the as-sprayed coating in comparison to those of the laser-assisted fusing treatment [21].

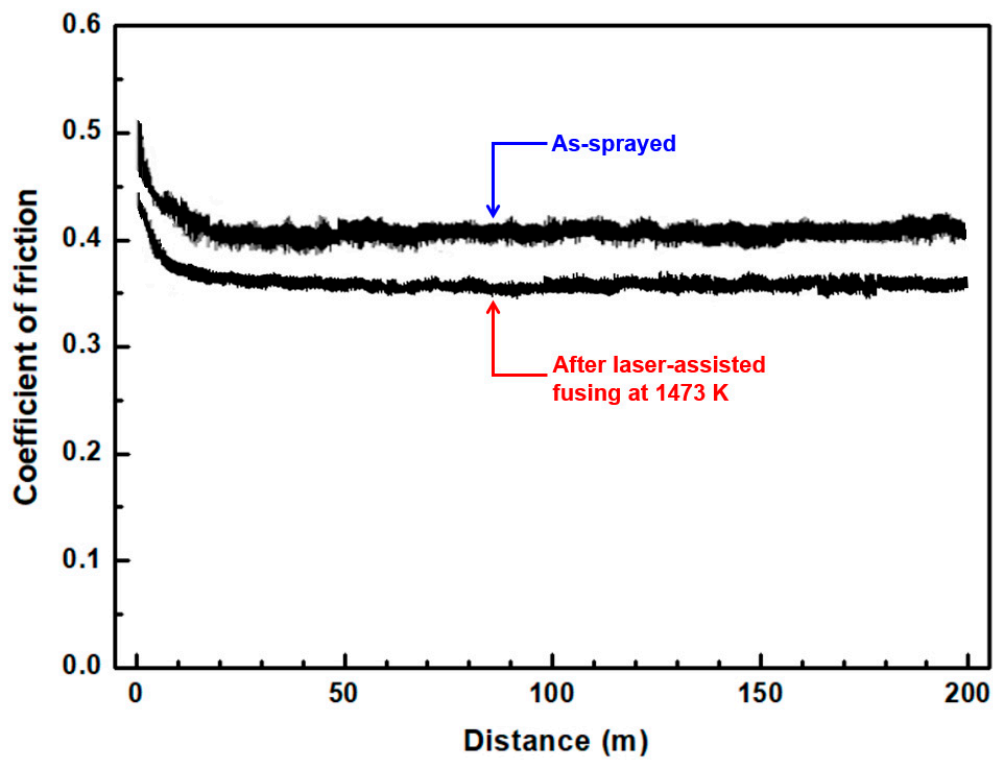


Figure 10. Comparison of coefficient of friction of thermal-sprayed 1276F coating and that after laser-assisted fusing at 1473 K.

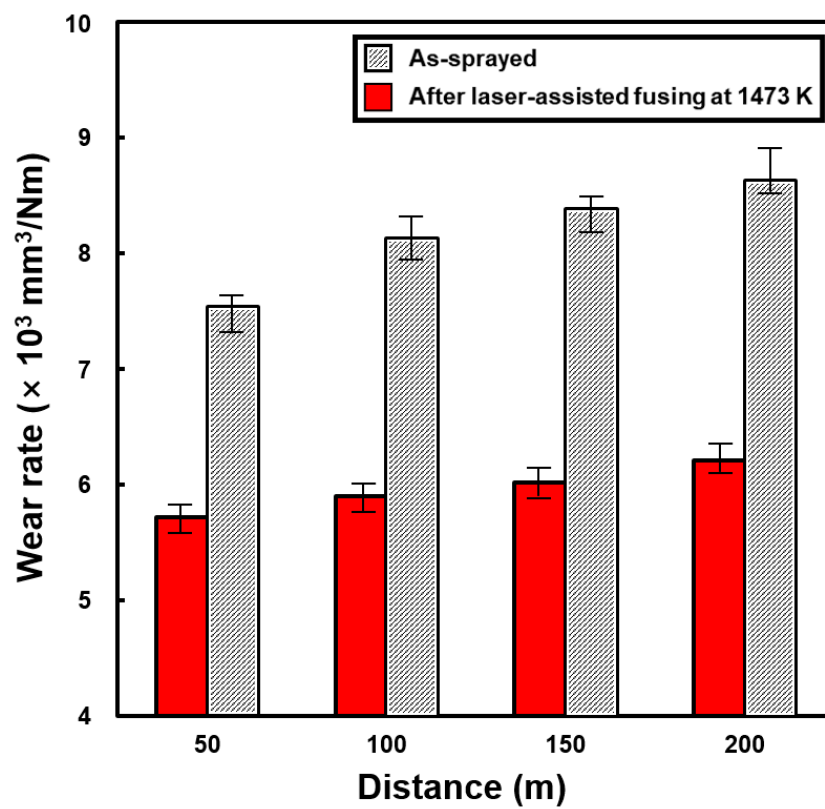


Figure 11. Comparison of average wear rate of thermal-sprayed 1276F coating and that after laser-assisted fusing at 1473 K.

Figure 12 shows the SEM images and line profilometries of the worn surface for the as-sprayed coating and laser-assisted fusing treatment after the tribotest. In the case of the as-sprayed coating, deep abrasion grooves and wear debris can be observed on the worn surface. On the other hand, a relatively smooth worn surface was obtained with the laser-assisted fusing coating. The line profile was obtained from perpendicular to the sliding direction (marked with white dot lines in figures) and relatively rougher line profile was observed for the as-sprayed coating than that of the laser-assisted fusing treatment. Moreover, the average roughness (R_a) was found to be $2.67\ \mu\text{m}$ for the as-sprayed coating and $1.44\ \mu\text{m}$ for the laser-assisted fusing coating. In other words, this surface roughness was well matched with the tribological performance, as described in Figures 10 and 11. The reason for the lower COF and wear rate of the laser-assisted fusing coating, relative to the as-sprayed coating, was speculated to be the increased surface hardness and the microstructural evolution (e.g., the homogeneous formation of fine carbides and borides), as described in Section 4.3.

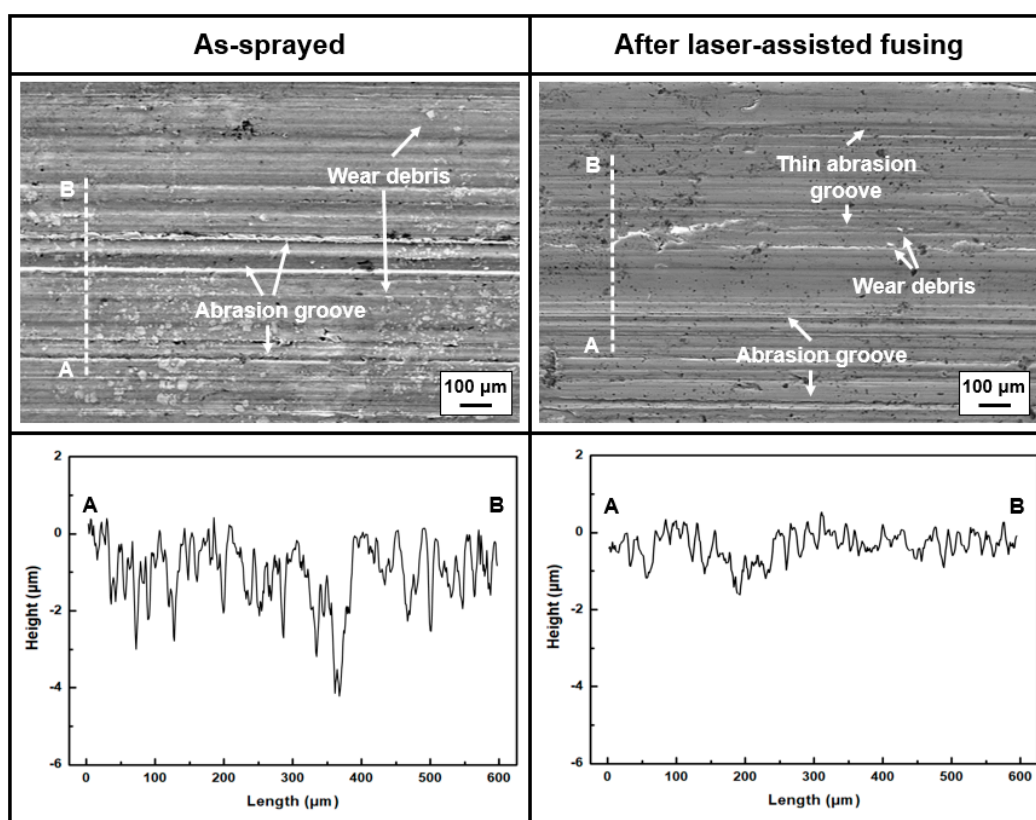


Figure 12. Surface morphology and line profile of worn surface of as-sprayed 1276F coating and that after laser-assisted fusing at 1473 K.

Figure 13 also shows the EPMA results for the worn surface of the as-sprayed 1276F coating. As shown in the secondary electron (SE) image, the region exhibiting the deeper wear marks is closely related to the region in which W is depleted, given that this element is required for the formation of carbides and borides. In other words, it could be concluded that this result is closely related to the larger variation in the COF value of the as-sprayed coating, as shown in Figure 10. Consequently, it follows that the laser-assisted fusing treatment densifies the microstructure to form secondary phases, thereby leading to the surface hardening of the HVOF-sprayed 1276F alloy coating. As a result, the tribological performance was successfully enhanced.

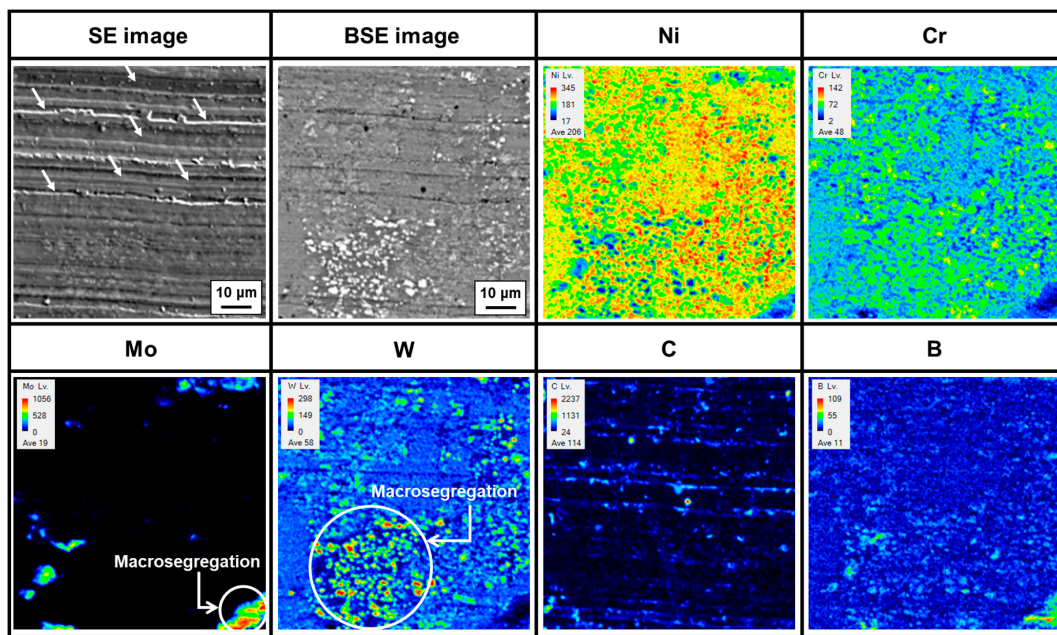


Figure 13. EPMA analysis for worn surface of as-sprayed 1276F coating.

6. Conclusions

In the present study, the applicability of laser-assisted fusing treatment was investigated for a 1276F thermal-sprayed alloy coating. High-power diode laser with temperature control were used for this treatment, which was intended to enhance the abrasion and erosion resistance of continuous-casting molds. The variation in the microstructure and hardness distribution, as well as the tribological performance were characterized. As a result, the following conclusions can be drawn:

- i. Based on the results of thermodynamic calculations, the temperature of the laser-assisted fusing was set to a range of 1173–1473 K; during the fusing treatment, this temperature was maintained using a pyrometer system. After the laser-assisted fusing treatment, imperfections such as the macrosegregation of certain alloying elements and voids were diminished, relative to the as-sprayed sample.
- ii. The zone subjected to fusing exhibited finely distributed secondary phases, which were not observed in the as-sprayed zone. These fine secondary phases (carbides and borides) were identified as $M_{23}C_6$, M_7C_3 and M_5B_3 , with sizes ranging from 0.05 to 10 μm , approximately. The hardness increment from 730 (as-sprayed status) to 1230 HV (at 1473 K) after the laser-assisted fusing treatment was attributed to the generation of these finely distributed carbides and borides.
- iii. The coating subjected to laser-assisted fusing exhibited greater wear resistance than that of the as-sprayed coating. The coefficient of friction and wear rate of the as-sprayed coating were both somewhat higher than those of the laser-assisted fusing coating. The superior tribological properties of the laser-assisted fusing coating, relative to the as-sprayed coating, were attributed to the increase in the surface hardness, as well as the microstructural homogeneity.

Author Contributions: Conceptualization, E.-J.C.; methodology, E.-J.C. and C.P.; software, E.-J.C.; formal analysis, C.P.; investigation, E.-J.C. and C.P.; writing—original draft preparation, E.-J.C. and C.P.; writing—review and editing, E.-J.C.; supervision, E.-J.C.; funding acquisition, E.-J.C. and C.P. All authors have read and agreed to the published version of the manuscript.

Funding: This work was supported by National Research Foundation, Republic of Korea (Project number: 2019R1G1A1099607) and the National Research Council of Science and Technology, Republic of Korea (Project number: NK226A, 2020).

Conflicts of Interest: The authors declare no conflict of interest.

References

1. Hamatani, H.; Ichiyama, Y.; Kobayashi, J. Mechanical and thermal properties of HVOF sprayed Ni based alloys with carbide. *Sci. Technol. Adv. Mater.* **2002**, *3*, 319–326. [[CrossRef](#)]
2. Matthews, S.; James, B. Review of thermal spray coating applications in the steel industry: Part 1– hardware in steel making to the continuous annealing process. *J. Therm. Spray. Technol.* **2010**, *19*, 1267–1276. [[CrossRef](#)]
3. Chen, H.; Su, L.; Wang, G.; Wan, S.; Zhang, L.; Luo, Z. Fuzzy estimation for heat flux distribution at the slab continuous casting mold surface. *Int. J. Therm. Sci.* **2014**, *83*, 80–88. [[CrossRef](#)]
4. Barella, S.; Gruttadauria, A.; Mapelli, C.; Mombelli, D. Investigation of failure and damages on a continuous casting copper mould. *Eng. Fail. Anal.* **2014**, *36*, 432–438. [[CrossRef](#)]
5. Shieh, Y.; Wang, J.; Shih, H.; Wu, S. Alloys and post-heat treatment of thermal sprayed coatings of self-fluxing alloys. *Surf. Coat. Technol.* **1993**, *58*, 73–77. [[CrossRef](#)]
6. Otsubo, F.; Era, H.; Kishitake, K. Structure and phases in nickel-base self-fluxing alloy coating containing high chromium and boron. *J. Therm. Spray Technol.* **2000**, *9*, 107–113. [[CrossRef](#)]
7. Otsubo, F.; Era, H.; Kishitake, K. Interface reaction between nickel-base self-fluxing alloy coating and steel substrate. *J. Therm. Spray Technol.* **2000**, *9*, 259–263. [[CrossRef](#)]
8. Sakata, K.; Nakano, K.; Miyahara, H.; Matsubara, Y.; Ogi, K. Microstructure control of thermally sprayed Co-based self-fluxing alloy coatings by diffusion treatment. *J. Therm. Spray Technol.* **2007**, *16*, 991–997. [[CrossRef](#)]
9. Houdková, Š.; Pala, Z.; Smazalová, E.; Vostřák, M.; Česánek, Z. Microstructure and sliding wear properties of HVOF sprayed, laser remelted and laser clad Stellite 6 coatings. *Surf. Coat. Tech.* **2017**, *318*, 129–141. [[CrossRef](#)]
10. Santhanakrishnan, S.; Kovacevic, R. Hardness prediction in multi-pass direct diode laser heat treatment by on-line surface temperature monitoring. *J. Mater. Proc. Technol.* **2012**, *212*, 2261–2271. [[CrossRef](#)]
11. Chun, E.J.; Sim, A.; Kim, M.S.; Kang, N. Microstructural characterization of surface softening behavior for Cu-bearing martensitic steels after laser surface heat treatment. *Metals* **2018**, *8*, 470. [[CrossRef](#)]
12. Shariff, S.M.; Pal, T.K.; Padmanabham, G.; Joshi, S.V. Influence of chemical composition and prior microstructure on diode laser hardening of railroad steels. *Surf. Coat. Technol.* **2013**, *228*, 14–26. [[CrossRef](#)]
13. Hongchao, Q. Experimental investigation of laser peening on Ti17 titanium alloy for rotor blade applications. *Appl. Surf. Sci.* **2015**, *351*, 524–530. [[CrossRef](#)]
14. Li, R.; Jin, Y.; Li, Z.; Qi, K. Comparative study of high-power diode laser and CO₂ laser surface hardening of AISI 1045 Steel. *J. Mater. Eng. Perform.* **2014**, *23*, 3085–3091. [[CrossRef](#)]
15. Soriano, C.; Leunda, J.; Lambarri, J.; Navas, V.G. Effect of laser surface hardening on the microstructure, hardness and residual stresses of austempered ductile iron grades. *Appl. Surf. Sci.* **2011**, *257*, 7101–7106. [[CrossRef](#)]
16. Qiu, F.; Uusitalo, J.; Kujanpaa, V. Laser transformation hardening of carbon steel: Microhardness analysis on microstructural phases. *Surf. Eng.* **2013**, *29*, 34–40. [[CrossRef](#)]
17. Giacomantonio, M.; Gulizia, S.; Jahedi, M.; Wong, Y.; Moore, R.; Valimberti, M. Heat treatment of thermally sprayed Ni-based wear and corrosion coatings. *Mater. Forum.* **2011**, *35*, 48–55.
18. Lugscheider, E.; Hofmann, D.; Nicoll, A.R. Optimization of spraying process and laser treatment of CoNiCrAlY. *J. Therm. Spray Technol.* **1992**, *1*, 239–247. [[CrossRef](#)]
19. Chun, E.J.; Kim, M.S.; Nishikawa, H.; Park, C.; Suh, J. Laser-assisted selective fusing of thermal sprayed Ni-based self-fluxing alloys by using high-power diode lasers. *Opt. Laser Technol.* **2018**, *100*, 317–324. [[CrossRef](#)]
20. Chun, E.J.; Park, C.; Nishikawa, H.; Kim, M.S. Microstructural characterization of Ni-based self-fluxing alloy after selective surface-engineering using diode laser. *Appl. Surf. Sci.* **2018**, *442*, 726–735. [[CrossRef](#)]
21. Grützmacher, P.G.; Rammacher, S.; Rathmann, D.; Motz, C.; Mücklich, F.; Suarez, S. Interplay between microstructural evolution and tribo-chemistry during dry sliding of metals. *Friction* **2019**, *7*, 637–650. [[CrossRef](#)]

